American Journal of Energy Research, 2021, Vol. 9, No. 1, 6-20
Available online at http://pubs.sciepub.com/ajer/9/1/2
Published by Science and Education Publishing
DOI:10.12691/ajer-9-1-2

A Thermal Node Model for Predicting Heat Transfer in Mixed Type Solar Drying System

Carine Pamela Aghogue Donchi[1,*], Ernest Léontin Lemoubou[1], Hervé Thierry Tagne Kamdem[1], René Tchinda[2]

[1]Life & Industrial Systems Thermal Engineering-Team (LISTE-T), Research Unit of Mechanics and Physical Systems Modeling (UR-2MSP), Department of Physics/Faculty of Sciences, University of Dschang, Dschang, Cameroon
[2]Institute of Technology Fotso-Victor Bandjoun, Bandjoun, Cameroon
*Corresponding author: pameladonchi91@gmail.com

Received February 21, 2021; Revised April 04, 2021; Accepted April 12, 2021

Abstract The present paper deals with an equivalent two-dimensional prediction of a mixed solar drying system performances using a thermal network procedure and the numerical simulation. The aim has been to build the equivalent electric circuit of the mixed solar drying facility and investigate the space and time variabilities of temperature transfer in a solar drying system.The balance equations modelling the physical elements are approximated iteratively using the finite difference method. The results obtained indicate that the proposed two-dimensional predictions based on sinusoidal approximation of solar radiation and air temperature inputs adequately describe both collector and dryer temperature profiles. The influences of various parameters such as the space resolution, the mass flow rate, the average temperature and solar radiation inputs have been investigated and discussed. The numerical simulations show that the temperature of each element of the drying system is not uniform and varies considerably with the space and time nodes, and therefore increases gradually from the first-node of the macroscopic drying flow to the end-node.

Keywords: *solar dryer, two-dimensional simulation, thermal node analysis, thermal performances*

Cite This Article: Carine Pamela Aghogue Donchi, Ernest Léontin Lemoubou, Hervé Thierry Tagne Kamdem, and René Tchinda, "A Thermal Node Model for Predicting Heat Transfer in Mixed Type Solar Drying System." *American Journal of Energy Research*, vol. 9, no. 1 (2021): 6-20. doi: 10.12691/ajer-9-1-2.

1. Introduction

The prediction of heat transfer in drying systems is very important in numerous engineering and lifetime domains. It is the key to improve preservation of agricultural crops for a long time period, to facilitate their transport and reduce agricultural losses after harvesting [1,2]. In fact, in order to prevent excessive agricultural losses after harvesting and improve thermal performance of solar dryers, mathematical and numerical modeling have recently been brought to bear on solar drying innovations such as to provide information on the course of drying in different conditions [3,4,5]. The information obtained may be used as a basis for optimization of the design and operating regime of such a system. It is therefore, important to formulate appropriate models and quantify mechanisms controlling solar drying for the performance evaluation and to describe fundamental parameters needed to understand the physical phenomena involved in the dryer for different configurations.

The first idea of solar dryer was developed during the past decades to avoid open sun drying problems [6,7]. The most historical method of using a solar energy for agricultural crops is the open sun drying also called traditional method of drying. The method consists to expose directly crops to solar radiation by spreading on the floor, on the mats or cemented surfaces, which expose them to bad weather [2,8]. To solve this problem, various types of solar dryers have been proposed to dry agricultural products around the world: direct solar dryer, indirect solar dryer, mixed-solar dryer, and hybrid solar dryer [3,5]. Several mathematical models like heat and mass balance models, thin-layer models, and equilibrium moisture content models have been developed to illustrate the dryer system for agricultural production [2,3,9]. Many researches have been made to improve the solar drying technology utilizing natural and forced circulation as well as the auxiliary electricity and fossil fuel source strategies [6]. Various methods have been adopted to improve the thermal performance of the solar air collector which is the most important element of the drying systems [10,11,12]. The single-pass solar air collector and the double-pass flow types are increasingly becoming operational [13,14]. The mass flow rate of the fluid as well as the position of the absorber are important factors that can affect the thermal performance of the solar collector. The compound parabolic concentrator having a flat one-sided absorber has been studied [15,16]. A double-pass solar dryer has shown to provide compatible results compared to standard dryers operated by electricity [17]. A tilted double-pass

natural convection solar tunnel air heater with in-built thermal storage attached with a tunnel dryer is one of the possible extension of the double pass air drying facilities. This type of dryer is very flexible for drying high moisture vegetables and other agricultural products. The use of staggered absorber sheets and attached fins on absorber surface with different shapes and dimensions is also appropriate to increase the efficiency of the collector [18]. However, these technics required an important initial investment. Optimizing the dimensions of the air heater construction elements and adopted sensible or latent storage media, concentrators to augment the available solar radiation, and integrating photovoltaic elements with the heaters, have been also reported [19,20]. The thermal and electrical analogies have been also employed to model solar systems [4]. The abovementioned applications of the solar air drying method indicated also that the investigation of the characterization of heat and mass transfer operating in the solar engineering system remains an active task for the researchers. In fact, the design and simulation of the processes occurred in the solar drying facility present great difficulties. Parameters variability of thermal properties on time and space variations as well as on temperature changes are one of the major problem of solar drying systems modeling. Most direct simulation models used in the approximations of thermal performance of the drying systems have been limited on one-dimensional transfer where changes in drying air velocity and temperature gradient are less sensitive to the transfer process. Important studies have presented also various models by assuming steady state transfer with fixed temperature and air velocity. Although these strategies can provide information on the characteristic curves of the solar drying systems, the results are still influenced by uncertainties in prediction accuracy and reliability. Therefore, more analyses are required to gain deeper knowledge of these systems especially with multi-dimensional test conditions.

The aim of this study is to make an assessment of the thermal characteristics of modelled drying facility with double air pass solar collector using the thermal node analysis. The main goal was to meet a detailed analysis of the spatial and temporal variabilities of temperature transfer in a solar drying system. For this purpose, the heat transfer process is described using a two-dimensional heat transfer model characterized with nonlinear conductive, convective and radiative properties. The input solar radiation and atmospheric temperature changes are performed using comprehensible sinusoidal models. The proposed solar drying model is configured using an electrical analogy based on the Kirchoff current law generally known as thermal network method. A system of twelve coupled nonlinear differential equations are obtained, and are solved iteratively using the finite difference approach. Based on this strategy, the computational responses of temperature transfer, energy and exergy distributions are generated as functions of space-time variations. The influence of the mass flow rate, the average temperature and solar radiation inputs are studied. Such analysis enables to display more representative interpretations on the temperature distribution of each important element of a thermal dryer.

2. Mathematical Model

2.1. Model Description of Collector and Drying Circuits

Real dryer consists of multidimensional system with nonlinear conductive, convective and radiative properties involved. Schematic diagrams of solar drying system is a structure of elementary nodes which are interconnected with capacity and resistance as shown in Figure 1. The dryer electrical system is configured with two major parts: the solar collector circuit and the dryer chamber circuit. This conceptualization has been already presented in the literature [2,4,8,13]. The inner dryer box is configured with aluminum sheet and the space between the outer box and inner tray including the bottom of the tray. The aforementioned components include clear glass cover of 3mm of thickness with dimensions $\boldsymbol{B} \times \boldsymbol{b}$, internal air, absorber plate, and the side plates. The outer box is considered to be built with plywood and has six mains pieces. In parallel, the solar collector is built with two passages: the first passage is formed between the aluminum plate of dimension $\boldsymbol{L} \times \boldsymbol{l}$ and absorber plate, and the second air flow zone between glass cover and the absorber plate. The cold air passes between the aluminum plate and the lower side of the absorber plate and then, flows between glass cover and the upper side of the absorber plate. The aluminum plate is supposed to have low thickness, high conductivity and it is black painted with greater absorption coefficient. The surfaces of absorber plate and glass cover are gray. Three heat transfer modes are considered to describe heat transfer processes during the drying processes: conduction, convection and radiation [21,22]. The glass absorbs part of incident radiation due to illumination from sun. It also receives heat energy from lower glass and then losses heat energy to ambient air. Similarly, the internal face of the glass cover receives heat by radiation from the base plate. It also receives the convection air from air enclosed. The absorber plate absorbs the incident solar radiation on it and losses the heat energy to air chamber by convection and to glass by radiation. The heat is also transferred to ambient milieu through the bottom and the side walls. The internal air receives the heat energy from absorber and losses heat energy to lower glass by convection. It also losses heat energy to side walls by convection process. The drying chamber consists of a chamber made of wood (outer layer) and aluminum (inner layer), above the drying room, an opening (chimney) which serves as an outlet for the air. These thermal heat transfer processes have been thoroughly described in several studies [5,11].

2.2. Thermal Network Equations

Following the analogy existing between thermal system and electrical circuit, the thermal network model for the system that composes the collector and the drying compartment can be seen in Figure 1. There are six nodes that represent the elements of the collector and six another nodes for the dryer chamber part, and these nodes are linked to another by thermal resistances; each resistance corresponding here to a particular type of heat transfer

(radiation, convection or conduction) between the different nodes. The equivalent electric circuits of the collector and dryer components are presented in Figure 2. The current nodal law states that the algebraic sum of current entering a node is zero of an electrical circuit. Implicitly, the algebraic sum of flux at each node of the constructed model is vanished. Applying the aforementioned approach on the equivalent network of Figure 2, the equivalent equations in each node of the thermal network are given in Table 1.

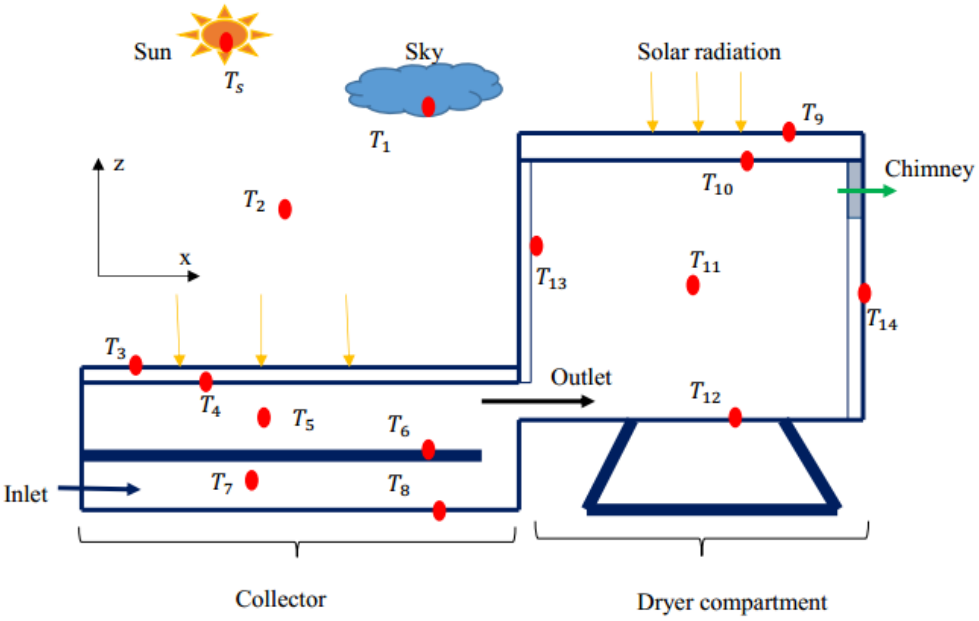

Figure 1. Schematic diagram of the mixed solar drying facility model

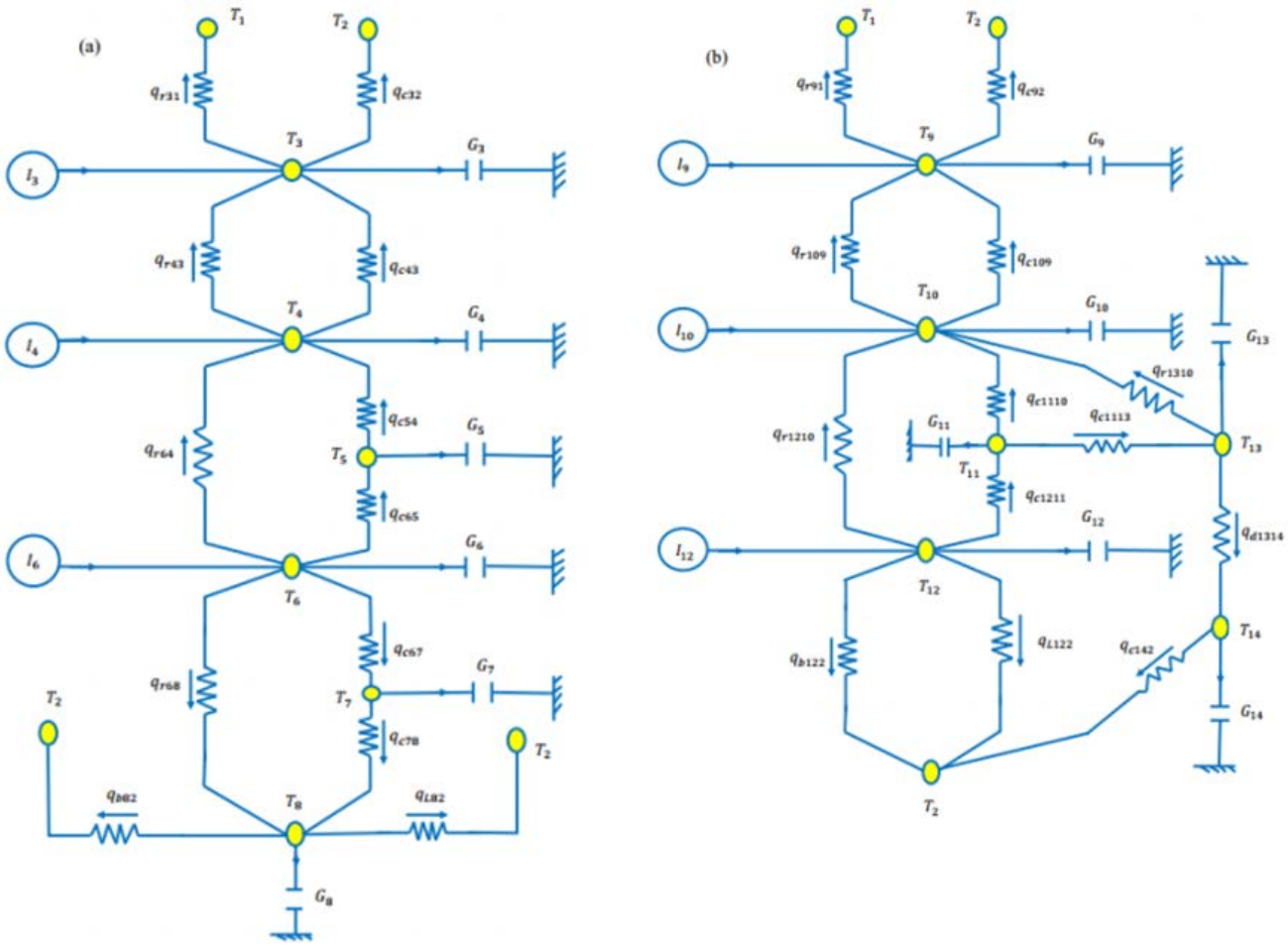

Figure 2. Thermal network of the solar collector (a) and solar dryer compartment (b)

Table 1. Description of the thermal drying system

Node	Description	Temperature	Equations
1	Sky	T_1	$T_1(t) = T_{2avr} + T_{2amp}\, sin\left[\omega\,(t-t_0)+\varepsilon_p\right] - 6$
2	Ambient	T_2	$T_2(t) = T_{2avr} + T_{2amp}\, sin\left[\omega\,(t-t_0)+\varepsilon_p\right]$
3	Glass cover 1	T_3	$I_3 + q_{r43} + q_{c43} - q_{c32} - q_{r31} - G_3 = 0$
4	Glass cover 2	T_4	$I_4 + q_{c54} + q_{r64} - q_{r43} - q_{c43} - G_4 = 0$
5	Air outlet	T_5	$q_{c65} - q_{c54} - G_5 = 0$
6	Absorber plate	T_6	$I_6 - q_{r64} - q_{c65} - q_{c67} - q_{r68} - G_6 = 0$
7	Air inlet	T_7	$q_{c67} - q_{c78} - G_7 = 0$
8	Aluminum plate	T_8	$q_{r68} + q_{c78} - q_{b82} - q_{L82} - G_8 = 0$
9	Glass cover 3	T_9	$I_9 + q_{r109} + q_{c109} - q_{c92} - q_{r91} - G_{10} = 0$
10	Glass cover 4	T_{10}	$I_{10} + q_{r1210} + q_{c1110} + q_{r1310} - q_{r109} - q_{c109} - G_{10} = 0$
11	Drying air	T_{11}	$q_{c1211} - q_{c1113} - q_{c1110} - G_{11} = 0$
12	Base plate	T_{12}	$I_{12} - q_{r1210} - q_{c1211} - q_{b122} - q_{L122} - G_{12} = 0$
13	Inner plate	T_{13}	$q_{c1113} - q_{c1310} - q_{d1314} - G_{13} = 0$
14	outer plate	T_{14}	$q_{d1314} - q_{c142} - G_{14} = 0$

For this model, q_{cij}, q_{rij} and q_{dij} are the convective flux, the radiative transfer flux and the conductive flux, and are approximated respectively by

$$q_{cij} = \frac{T_i - T_j}{\frac{1}{h_{cij}S_i}},\ q_{rij} = \frac{T_i - T_j}{\frac{1}{h_{rij}S_i}},\ q_{dij} = \frac{T_i - T_j}{\frac{e_{ij}}{h_{dij}S_i}},\ i \neq j, \quad (1)$$

where $T_i = T_i(x,y,t)$ is the temperature of the element i, and h_d, h_c, and h_r represent the conductive heat transfer coefficient, the convective coefficient, and the radiative coefficient, respectively. The quantities $1/\left(h_{cij}S_i\right)$, $1/\left(h_{rij}S_i\right)$, and $e_{ij}/\left(h_{dij}S_i\right)$ are surface resistances of the abovementioned heat transfer phenomena. The storage flux G_i during the time Δt is expressed as

$$G_n = \frac{T_n^{k+1}(i,j) - T_n^k(i,j)}{\frac{\Delta t}{m_n c_{pn}}},\ n \neq 5,7,11; \quad (2)$$

and

$$G_n = \frac{T_n^{k+1}(i+1,j) - T_n^{k+1}(i,j)}{\frac{\Delta x}{Qc_{pn}}} + \frac{T_n^{k+1}(i,j+1) - T_n^{k+1}(i,j)}{\frac{\Delta y}{Qc_{pn}}},\ n = 5,7,11. \quad (3)$$

In which m_n, c_{pn}, T_n, S_n and Δt represent the mass, the specific heat capacity and the temperature of element n of the drying system or the node temperature, the surface, and the time step, respectively. In this study, the thermal capacitance of the working fluid was neglected.

The global surface fluxes I_3, I_4 and I_6 give the rate of the solar intensity that reaches the external glass cover, the internal glass cover and the absorber plate of the collector, respectively. The fluxes I_{10}, I_9, and I_{12} have the same meanings but identify the dryer chamber components. These fluxes can be written as

$$I_3 = \alpha_3 I S_3,\ I_4 = \tau_3\alpha_4 I S_4,\ I_6 = \tau_3\tau_4\alpha_6 I S_6,\ I_9 = \alpha_9 I S_9,\ I_{10} = \tau_9\alpha_{10} I S_{10},\ I_{12} = \tau_9\tau_{10}\alpha_{12} I S_{12} \quad (4)$$

where I is the global solar radiation, α_i is the absorptivity coefficient, and τ_i is the transmissivity of element i.

The global equations can be written as

$$\frac{m_3 c_{p3}}{S_3}\frac{dT_3}{dt} = \alpha_3 I + h_{r4\_3}(T_4 - T_3) + h_{c4\_3}(T_4 - T_3) + h_{c3\_2}(T_2 - T_3) + h_{r3\_1}(T_1 - T_3), \quad (5)$$

$$\frac{m_4 c_{p4}}{S_4}\frac{dT_4}{dt} = \tau_3\alpha_4 I + h_{c5\_4}(T_5 - T_4) + h_{r6\_4}(T_6 - T_4) + h_{r4\_3}(T_3 - T_4) + h_{c4\_3}(T_3 - T_4), \quad (6)$$

$$\frac{Qc_{p5}}{l}\frac{dT_5}{dx} = -\frac{Qc_{p5}}{L}\frac{dT_5}{dy} + h_{c6\_5}(T_6 - T_5) + h_{c5\_4}(T_4 - T_5), \quad (7)$$

$$\frac{m_6 c_{p6}}{S_6}\frac{dT_6}{dt} = \tau_3\tau_4\alpha_6 I + h_{r6\_4}(T_4 - T_6) + h_{c6\_5}(T_5 - T_6) + h_{c6\_7}(T_7 - T_6) + h_{r6\_8}(T_8 - T_6) \quad (8)$$

$$\frac{Qc_{p7}}{l}\frac{dT_7}{dx} = -\frac{Qc_{p7}}{L}\frac{dT_7}{dy} + h_{c6\_7}(T_6 - T_7) + h_{c7\_8}(T_8 - T_7), \quad (9)$$

$$\frac{m_8 c_{p8}}{S_8}\frac{dT_8}{dt} = h_{r6\_8}(T_6 - T_8) + h_{c7\_8}(T_7 - T_8) + h_{b8\_2}(T_2 - T_8) + h_{L8\_2}(T_2 - T_8), \quad (10)$$

$$\frac{m_9 c_{p9}}{S_9}\frac{dT_9}{dt} = \alpha_9 I + h_{r10\_9}(T_{10} - T_9) + h_{c10\_9}(T_{10} - T_9) + h_{r9\_1}(T_1 - T_9) + h_{c9\_2}(T_2 - T_9), \quad (11)$$

$$\frac{m_{10}c_{p10}}{S_{10}}\frac{dT_{10}}{dt}=\tau_9\alpha_{10}I+h_{r12\_10}\left(T_{12}-T_{10}\right)+h_{c11\_10}\left(T_{11}-T_{10}\right)+h_{r13\_10}\left(T_{13}-T_{10}\right)+h_{r10\_9}\left(T_9-T_{10}\right)+h_{c10\_9}\left(T_9-T_{10}\right), \quad (12)$$

$$\frac{Qc_{p11}}{b}\frac{dT_{11}}{dx}=-\frac{Qc_{p11}}{B}\frac{dT_{11}}{dy}+h_{c12_{11}}\left(T_{12}-T_{11}\right)+h_{c11_{13}}\left(T_{13}-T_{11}\right)+h_{c11_{10}}\left(T_{10}-T_{11}\right), \quad (13)$$

$$\frac{m_{12}c_{p12}}{S_{12}}\frac{dT_{12}}{dt}=\tau_9\tau_{10}\alpha_{12}I+h_{r12\_10}\left(T_{10}-T_{12}\right)+h_{c12\_11}\left(T_{11}-T_{12}\right)+h_{b12\_2}\left(T_2-T_{12}\right)+h_{L12\_2}\left(T_2-T_{12}\right), \quad (14)$$

$$\frac{m_{13}c_{p13}}{S_{13}}\frac{dT_{13}}{dt}=h_{c11\_13}\left(T_{11}-T_{13}\right)+h_{r13\_10}\left(T_{10}-T_{13}\right)+h_{d13\_14}\left(T_{14}-T_{13}\right), \quad (15)$$

$$\frac{m_{14}c_{p14}}{S_{14}}\frac{dT_{14}}{dt}=h_{d13\_14}\left(T_{13}-T_{14}\right)+h_{c14\_2}\left(T_2-T_{14}\right). \quad (16)$$

In which the coefficients h_b and h_L are the heat loss coefficients of the base backside and wall backside insulation in the solar collector.

2.3. Thermal Transfer Functions

The conductive, radiative and convective transfer functions are fundamental to temperature and air flow in a solar system. In the network built in this study, the previous coefficients vary with the temperature changes. As stated before, the flow regime considered is natural convection. All conductive, convective and radiative heat transfer coefficients used here can be found in [11]. Therefore, the radiative heat transfer coefficient between the external glass cover and sky is given as

$$h_{r3\_1}=\varepsilon_3\sigma\left(T_3^2+T_1^2\right)\left(T_3+T_1\right). \quad (17)$$

The coefficient h_{r1_9} are calculated in the same manner. The radiation heat transfer coefficient between the external and internal glass cover is given by:

$$h_{r4\_3}=\frac{\sigma\left(T_3^2+T_4^2\right)\left(T_3+T_4\right)}{\frac{1}{\varepsilon_3}+\frac{1}{\varepsilon_4}-1}. \quad (18)$$

The radiation heat transfer coefficient between the internal glass cover and the absorber plate or the coefficient between the absorber and aluminum plate were evaluated in the same manner.

The convective transfer coefficient between the plate and fluid was obtained from Duffie and Beckman and given by [23].

$$h_{c6\_5}=\frac{\kappa_{6\_5}Nu_{6\_5}}{e_{6\_5}}, \quad (19)$$

where Nu_{6_5} is the Nusselt number.

The physical properties of the air were taken at medium temperature. On the other hand, the wind speed coefficient h_{3_2} or h_{9_2} is expressed as

$$h_{c3\_2}=5.7+3.8U, \quad (20)$$

where, U represents the wind speed.

3. Initial, Boundary Conditions and Numerical Implementation

The main drawback of the solar drying system is the complexity of the resulting equations. These partial differential equations are highly nonlinear because of the coupling of theses equations and the heterogeneity of the physical functions, which describe the relation between the temperature and the thermal properties. Therefore, solving the collector and dryer equations defined by Eqs. (5-16) for heat transfer problem requires appropriate formulation of initial and boundary conditions. In this study, the atmospheric boundary is fitted using the sinusoidal models. The air temperature can be expressed as

$$T_2\left(t\right)=T_{2avr}+T_{2amp}\sin\left[\omega\left(t-t_0\right)+\varepsilon_p\right], t\geq 0 \quad (21)$$

and the solar radiation by

$$I\left(t\right)=I_{avr}+I_{amp}\sin\left[\omega\left(t-t_0\right)+\varepsilon_p\right], t\geq 0, \quad (22)$$

where T_{2avr} is the average ambient temperature, T_{2amp} is the amplitude of temperature transfer, I_{avr} is the average solar intensity, I_{amp} is the amplitude of the solar intensity, $\omega=2\pi/\tau_0$ is the frequency, τ_0 is the period of the thermal wave, and $\varepsilon_p=\pi/2$ is the phase shift that depends on the time started point. This model is very flexible since by mean of average temperature and solar radiation, the influence of measuring these meteorological variables at a set of difference conditions can be applied. Therefore, in a real case, the presented equations will not hold perfectly the estimation of solar variables, but only provide approximate solution so that the characteristic profiles must be regarded being affected by some errors that typically occur during calibration and field measurements.

The initial condition for all temperatures is set at the heated values computed at the second time nodes. In addition, when the zero flux boundary type is assumed at the four sides of the collector and dryer parts of the studied system,

$$\left.\frac{\partial T}{\partial x}\right|_{x=0}=\left.\frac{\partial T}{\partial y}\right|_{y=0}=\left.\frac{\partial T}{\partial x}\right|_{x=l}=\left.\frac{\partial T}{\partial y}\right|_{y=b}=\left.\frac{\partial T}{\partial x}\right|_{x=L}=\left.\frac{\partial T}{\partial y}\right|_{y=B}=0. \quad (23)$$

In case of constant temperature assumed at the four sides of the system, one can write

$$T\big|_{x=0} = T\big|_{y=0} = T\big|_{x=l} = T\big|_{y=b} = T\big|_{x=L} = T\big|_{y=B} = T_2(t). \quad (24)$$

The numerical integration of these nonlinear model equations required a systematic iterative procedure. Several numerical procedures for one dimensional heat transfer in a solar drying system have been described in the literature [9,22]. The discrete forms of various heat transfer equations were approximated using the implicit finite difference procedure implemented in MATLAB computer language. In such case, the computations were accomplished along the *x* and *y* directions of the air flow in the considered system. In the numerical calculations, the iterative computation similar to the Gauss Seidel iteration was adopted to solve the complete time discretized equations such as to take naturally into account the effect of the temperature dependence of the various heat transfer coefficients. In such a method, the temperature field $T(x,y,t)$ is discretized at space node as $T_{i,j}^{k+1,m+1}$ in which the subscript (i,j) indicates the position in the finite difference mesh, while the superscript *k* and *m* represent time step and iteration level, respectively. Numerical simulations were initiated assuming the preheated aspect of temperatures of the various elements of the drying system. The adopted scheme allows iterative computation of the discretized system at each time step. Iteration continues until the specified iteration criterion is achieved. The criterion limit of the computational solution was achieved when the relative error between the maximum of calculated unknown values of temperature at two consecutive iteration levels is less than 10^{-6}.

4. Energy and Exergy Calculations

The general expressions of exergy and energy balances for solar system have been expressed in many researches [19,24]. The amount of the energy received by solar collector is given in function of the total collector area $A_6 = l \times L$ and the global solar radiation that reaches the collector.

$$I_{s_{en\_in}} = \tau_3 \tau_4 \alpha_6 I A_6. \quad (25)$$

On the other hand, the output energy shows itself as the increase in energy that the air has due to the temperature growth.

$$I_{s_{en\_out}} = Q c_{p5} (T_{5\_out} - T_{5\_in}). \quad (26)$$

The instantaneous efficiency $\eta_{en} = I_{s_{en\_out}} / I_{s_{en\_in}}$ measures the ratio of the useful heat gain transferred from the collector absorption plate to the working fluid to the total energy incident on the collector [10].

The input exergy to the collector and output exergy of solar system need to be determined. The input exergy can be evaluated as

$$I_{s_{ex\_in}} = I_{s_{en\_in}} \left[1 + \frac{1}{3}\left(\frac{T_2}{T_s}\right)^4 - \frac{4}{3}\frac{T_2}{T_s} \right]. \quad (27)$$

The surface temperature of the sun T_s is assumed to be $5800K$. The exergy output of the solar collector due to rise in air temperature can be expressed as

$$I_{s_{ex\_out}} = I_{s_{en\_out}} - Q c_{p5} T_2 \ln\left(\frac{T_{5_{out}}}{T_{5_{in}}}\right). \quad (28)$$

The exergy efficiency $\eta_{ex} = I_{s_{ex\_out}} / I_{s_{ex\_in}}$ is function of initial temperature and final temperature of the air and of the ambient temperature.

5. Results and Discussion

5.1. Validation of the Numerical Results

The accuracy of the numerical simulation is first validated by comparing the prediction of the heated air temperature solutions generated with the here presented model and the results of [25]. The parameters used are given in Table 2. For this simulation, the wind speed was setting at 1.5m/s, the daily solar radiation was setting at 600W/m^2 and the initial value of 30.98°C was used for the input air temperature. The flux type boundary conditions defined at all the sides of the drying facility were used.

Table 2. Major parameters used in the numerical Simulation

Parameters	Values	References
Wind speed	1.5 m/s	[25]
Air density	1.204kg/m^3	[30]
Boltzmann constant	5.67×10^{-8}	[23]
Glass cover		
Specific heat of glass cover	840 J/kg °C	[31]
Emissivity of glass cover	0.9	[11]
Transmittance of glass cover	0.84	[23]
Glass cover thickness	3mm	[7]
Glass cover absorptivity	0.06	[11]
Density of glass cover	2700 kg/m^3	[27]
Conductivity of glass	1.3 W/m °C	[27]
Absorber plate material	Aluminium painted in black	
Absorber plate thickness	1mm	[25]
Absorber plate absorptivity	0.95	[11]
Density of absorber plate material	2740 kg/m^3	[2]
Specific heat of absorber plate	896 J/kg °C	[2]
Emissivity of absorber plate	0.94	[12]
Insulation material	Glass wool covered	
Glass wool thickness	20mm	[28]
Plywood thickness	18mm	[11]
Conductivity of glass wool	0.04 W/m °C	[28]

Figure 3a shows the prediction accuracy of the heated air temperature in the collector. As can be seen in Figure 3b, the results of the proposed model are consistent. The simulated results provide the collector air temperature profile with a reasonable degree of accuracy. The maximum absolute error between the numerical prediction and the experimented curve is less than 2°C. For large heated time, especially for time greater than 11hr, this error is roughly equal to 1°C.

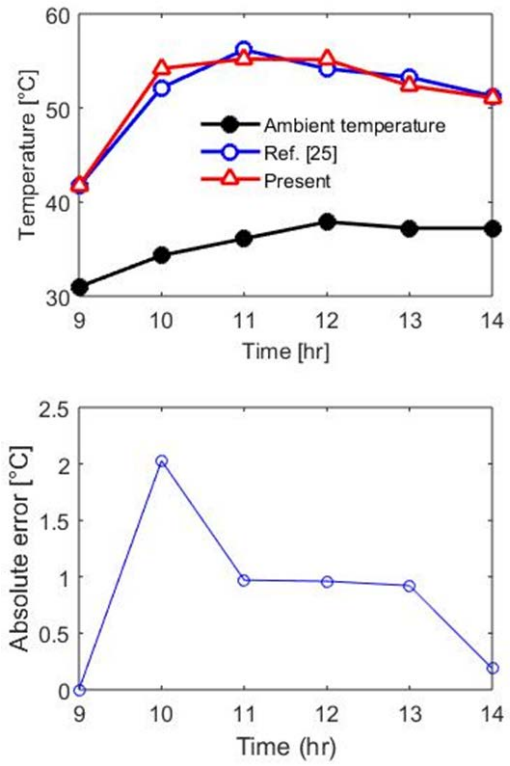

Figure 3. Validation of predicted collector air temperature with the results obtained by Gatea [25]

5.2. Time and Space Variabilities of the Temperature, Energy and Exergy of the Drying System

In the numerical simulations performed in this study, the sets of air temperature and solar radiation changes were simulated using the sinusoidal models presented by Eqs. (21) and (22), with the maximum solar radiation intensity 550W/m^2 and the average value of temperature input of 25°C and, the wind speed of 1.5m/s. In this simulation, a preheated system was considered and the results were obtained by using the physical parameters presented in Table 2. The solar dryer characteristic parameters used are very similar to that for literature [5,11]. The dimensions of the collector box used were $2m \times 1m$, while that of the drying chamber were $1m \times 1m$ but with $1m$ height.

Figure 4 depicts a three-dimensional distribution of temperature of external glass cover (T_3), internal glass cover (T_4), outer air (T_5), absorber plate (T_6), inner air (T_7), and aluminium plate (T_8). These results were computed using a period of the thermal wave $\tau_0 = 10hr$. It comes from this simulation that the temperatures of all collector elements increase gradually with the time and space node. In fact, at $x = 1.6m$, $y = 0.5m$ of the collector length, the range of the glass cover temperature was 25-34°C, while the internal glass cover reaches a maximum value of 37°C. The range of the absorber plate temperature was 45-135°C, while the inner air temperature varies from 26 to 65°C, and the average temperature of the drying cabinet varies from 35.5 to 64°C. In addition, as can be observed in Figure 5, the heated air temperature represented at $x = [0.4, 0.8, 1.6]m$ and for $y = 0.5m$, indicates clearly that the estimated temperatures at these positions do not have the same profile. Moreover, the ranges of the instantaneous energy and exergy efficiencies inside the dryer system are shown in Figure 6. The energy range in the dryer was decreased from 52% to 11%, while the exergy efficiency range was from 3.8% to 0.3%.

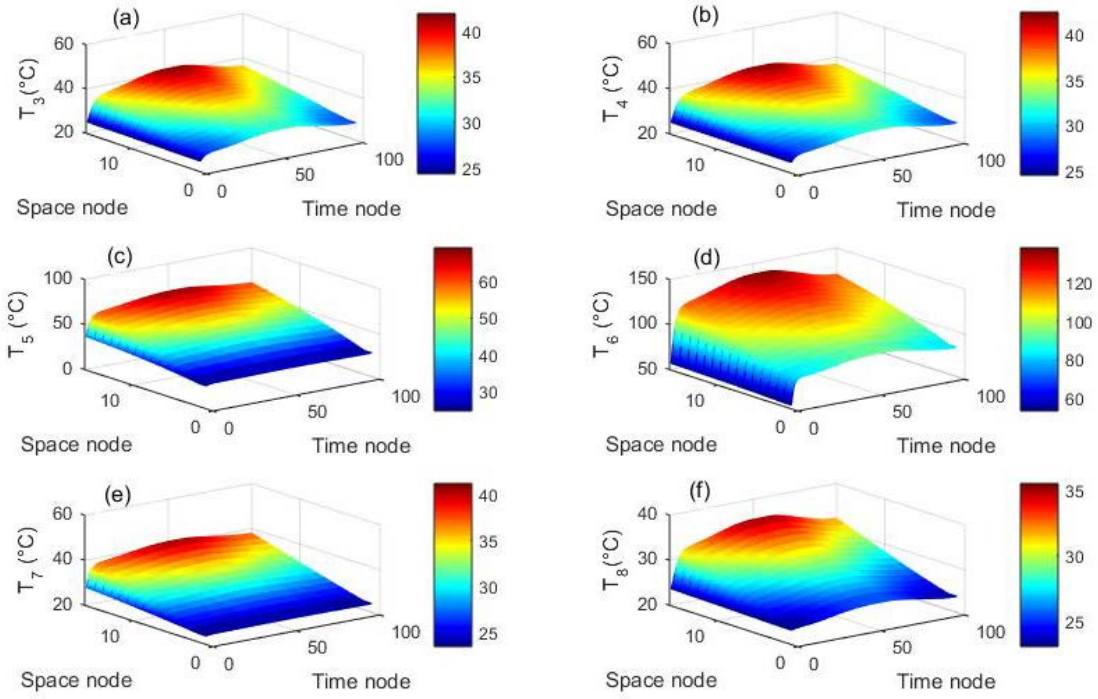

Figure 4. Three dimensional distribution of temperature of each element of the solar collector for τ_0=10hr: (a) external glass cover, (b) internal glass cover, (c) outer air, (d) absorber plate, (e) inner air, and (f) aluminium plate

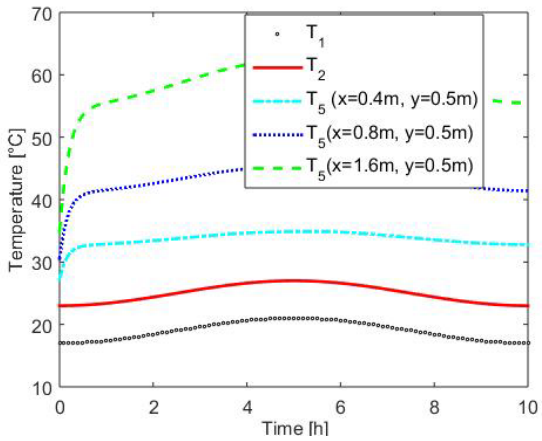

Figure 5. Potential distribution of the heated air temperature (T_5) at different x-position of the collector compared to the sky temperature (T_1) and ambient temperature (T_2)

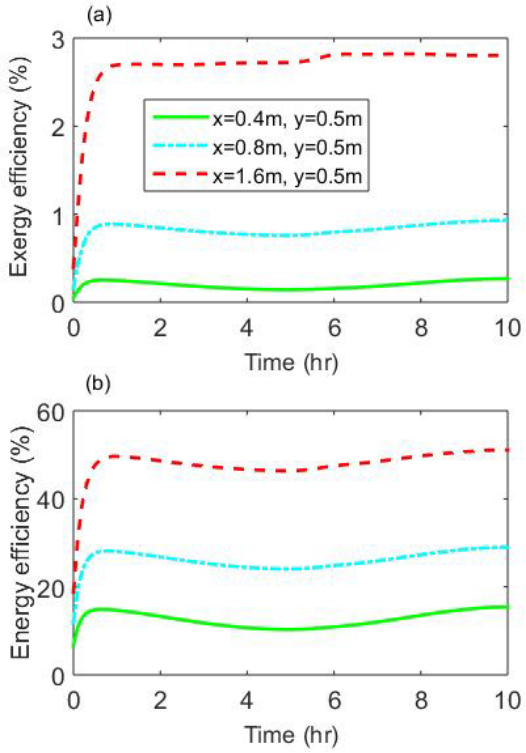

Figure 6. Comparison of the instantaneous exergy (a) and energy (b) efficiencies at different positions of the solar collector

Figure 7 shows the temperature profiles of each element of the solar dryer chamber for $\tau_0 = 5hr$. Therefore, the time and node variations of the temperature of external glass cover (T_9), internal glass cover (T_{10}), drying air (T_{11}), absorber plate (T_{12}), inner plate (T_{13}), and outer plate (T_{14}) are shown. Since the working fluid temperature changes significantly along the collector length of the dryer, the temperature distribution of other components of the dryer circuit must necessary be different. However, the modelled drying facility chamber temperature of each constituted elements exhibits the reverse temperature variation compared to the results of the collector elements presented in Figure 4. The prediction values of the temperature response computed at $t = 10hr$ show that the drying air temperature decreases from 68 to $48°C$. In parallel, the internal and external glass covers give relatively similar variation. The temperature of the internal face of the aluminium plate T_{13} is very low because the solar radiation does not reach this side of the dryer chamber while the reflection from the base plate has been neglected. In addition, for small time variations, the ambient temperature causes relatively a small variation between the outer wall temperature (T_{14}) and the inner plate temperature (T_{13}), afterward there is a slight increase of temperature of the inner plate due to the high conductivity of aluminum. It can be concluded that time and node variations have non-negligible effects on the temperature distribution of each element of the drying system.

For a period of the temperature wave equal to $\tau_0 = 3hr$, the results of temperature variations of the collector components, the dryer chamber elements, and the corresponding three dimensional distribution of the performances of the collector system are presented in Figure 8, Figure 9, and Figure 10, respectively. The synthetic tests give comparatively excellent agreement. As observed previously, considerable variabilities of the solar drying system temperature with the space and time are noted. The absorber plate temperature T_6 exhibits high maximum value, indicating greater effects on the model output, while their dynamic variation with the time node and space node (Figure 8) suggest nonlinear model response to input thermal wave changes. Still in Figure 8, the temperature of the aluminum plate T_8 is low compared to that of the absorber because of its low absorptivity. Subsequently, the high temperature of the absorber causes an increase in the temperature T_5 of the outlet air of the collector and therefore that of the inlet air in the collector channel T_7. According to Figures 8 and 9, a decrease of the outlet air temperature with the space node makes decreasing the instantaneous energy and exergy efficiency values. This observation can be justified by the fact that energy and exergy are function of initial and final temperatures of the air in the thermal facility system and also depend highly of the ambient temperature. Moreover, comparing Figure 10 and Figure 6, it appears that the exergy efficiency is considerably lower compared to the energy efficiency. In fact, the maximum exergy is around 4%, while the maximum values of 52% is obtained for the energy efficiency. It is important to mention here that the exergy efficiency is weak because of the irreversibility taking place in the solar collector. This last finding is in concordance with previous computations performed by [26] for a single glass cover solar collector, which indicated that for a mass flow rate of 0.012kg/s, the thermal efficiency varies from 40.02% to 51.50%.

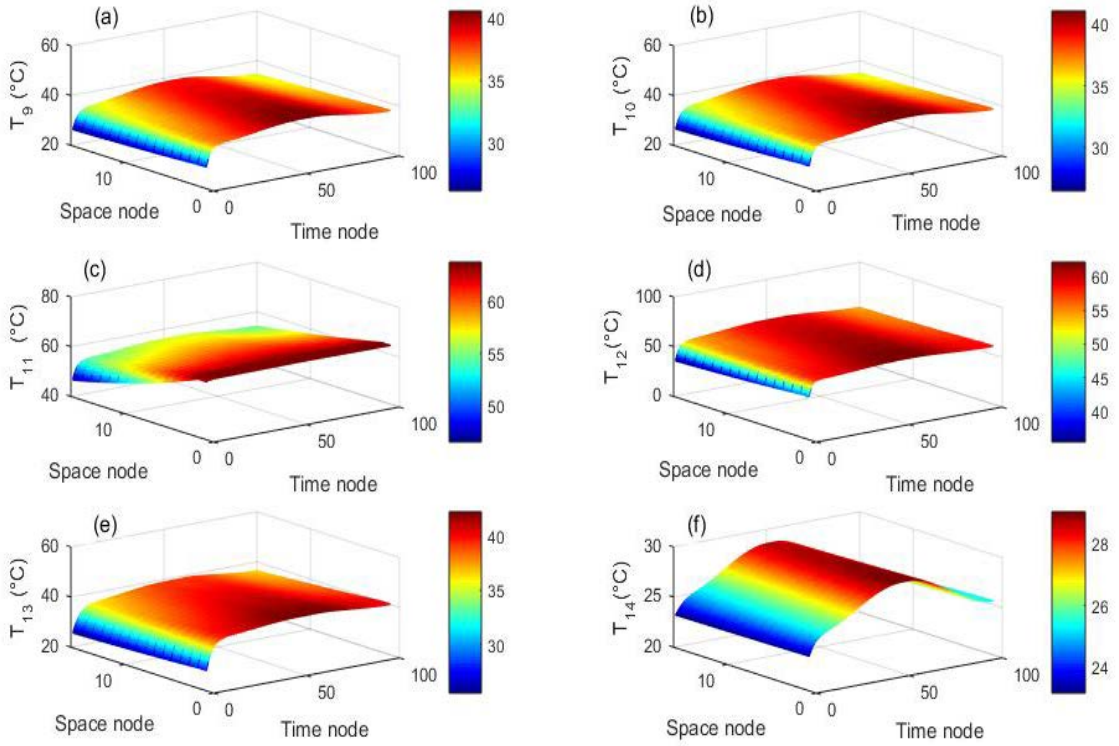

Figure 7. Three dimensional distribution of temperature of each element of the solar dryer chamber for τ_0=5*hr*: (a) external glass cover, (b) internal glass cover, (c) drying air, (d) absorber plate, (e) inner plate, and (f) outer plate

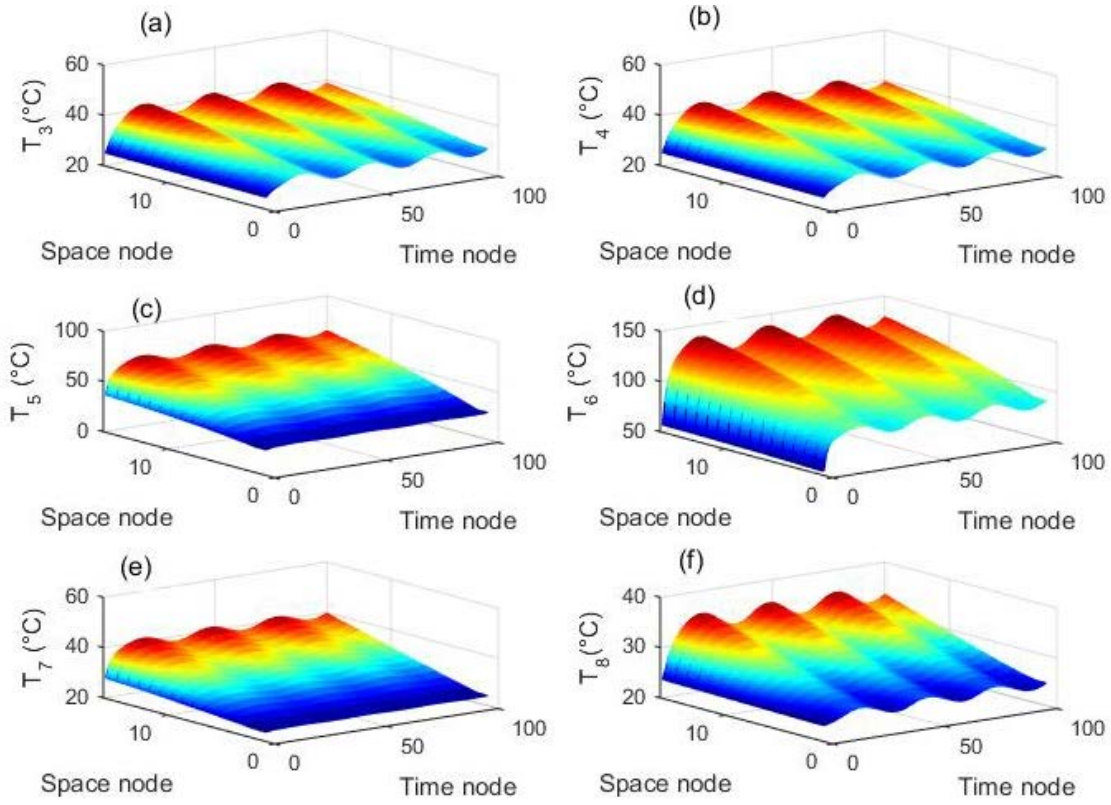

Figure 8. Three dimensional distribution of temperature of each element of the solar collector for τ_0=3*hr*: (a) external glass cover, (b) internal glass cover, (c) outer air, (d) absorber plate, (e) inner air, and (f) aluminium plate

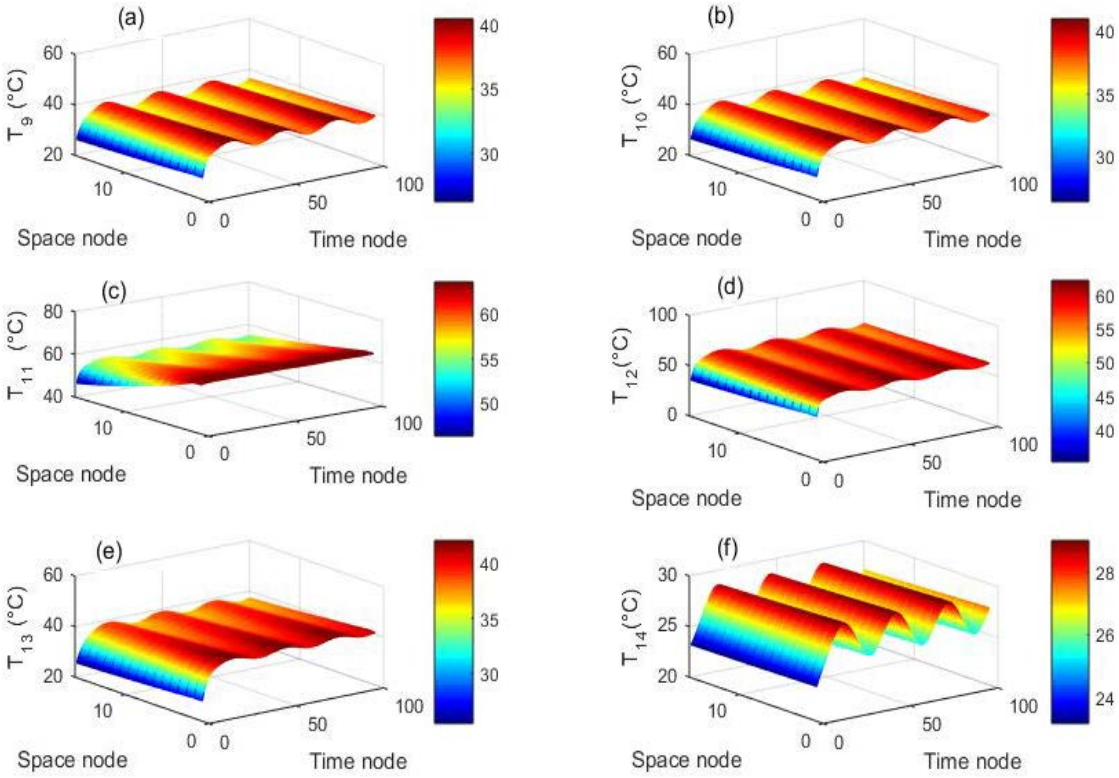

Figure 9. Three dimensional distribution of temperature of each element of the solar dryer chamber for τ_0=3*hr*: (a) external glass cover, (b) internal glass cover, (c) drying air, (d) absorber plate, (e) inner plate, and (f) outer plate

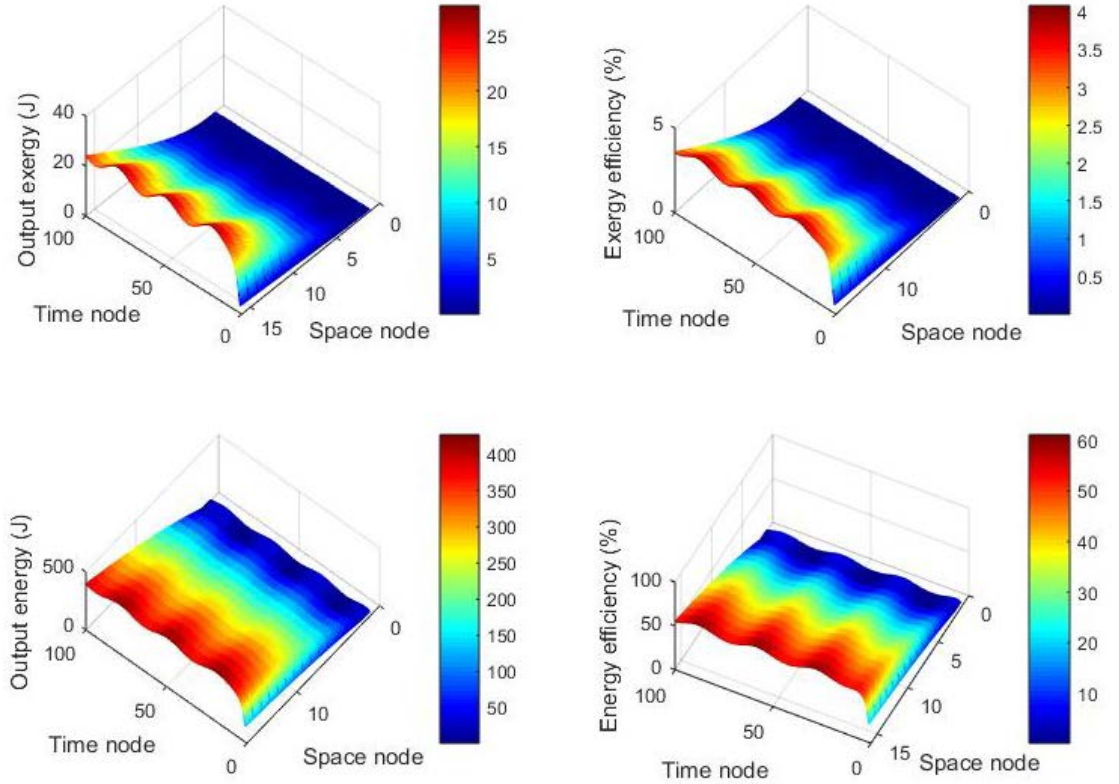

Figure 10. Three-dimensional view of the output exergy and energy, and the corresponding exergy and energy efficiencies

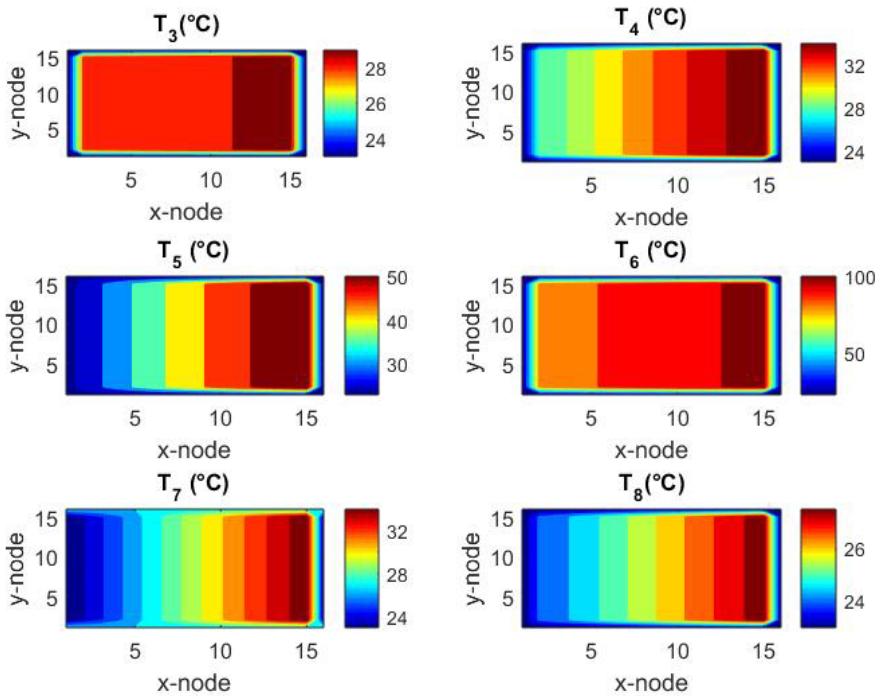

Figure 11. Two-dimensional distribution of temperature of external glass cover (T_3), internal glass cover (T_4), outlet air (T_5), absorber plate (T_6), inlet air (T_7), and aluminium plate (T_8) of the collector

5.3. Two-dimensional Spatial Variation of the Temperature Profile in the Drying Facility

In this section, the same prevailing simulation conditions of the previous synthetic examples described above were used. About the number of simulation nodes, 16×16 nodes were used and the solution is presented at $t = 5hr$. The case of Dirichlet boundary condition imposed at the four sides of the collector elements was considered. From Figure 11, it is observed that the peak temperature of the glass cover was $30°C$, while the internal glass cover reached a maximum value of about $33°C$. The absorber plate temperature achieved $100°C$, while the inner air temperature reached $50°C$, and the maximun temperature of the inlet channel reaches $33°C$. In addition, the low value of the aluminium plate temperature $(30°C)$ can be explained by the fact that the direct solar radiation does not illuminate the bottom wall of the collector cabinet. In addition, the output contour responses of Figure 11 clearly indicate that if the absorber plate temperature increases in the collector compartment with the space variation, the operating fluid temperature directly increases. The temperature variations of all components are relatively high especially at large nodes through the direction of the collector length, whereas slight differences appear at the initially steps of the solar air temperature changes. This can be justified by the fact that a dynamic behavior of air flowing through the channel should necessary damp the temperature histories of other parts of the thermal system. Thus, the amount of energy in each element of the dryer depends on the space node and is influenced by the air direction; the evaluation of the thermal performances of such a system must account it spatial variability.

5.4. Effect of Solar Intensity, Average Temperature Input, and Mass Air Flow Rate on the Variation of the Temperature Profiles, Energy and Exergy Efficiencies.

The effect of solar intensity input is analyzed in Figure 12. For this scenario, the average air temperature was $25°C$ while the air mass flow rate was set to $0.01kg/s$. The prediction was computed at position $(x, y) = (1.6, 0.5)m$ in the collector and $(x, y) = (0.8, 0.5)m$ in the dryer compartment.The sensitivity analysis was performed to study the effect of solar intensity, inner air speed and temperature boundary condition on the thermal performance of the collector. The results from Figure 12 show that the drying temperature transfer rate increases with increasing the average solar radiation coefficient. In parallel, the efficiencies decrease with decreasing solar radiation intensity.

Figure 13 depicts the effect of average temperature input on the thermal performance of the solar drying system. For this scenario, the solar intensity was kept constant and equal to $550W/m^2$ and the results were simulated for $T_{2avr} = \{20, 25, 30, 35\}°C$. From this investigation, it can be seen that the temperature of the studied model increases with the average ambient temperature. However, the results of the efficiency curves indicate that the increase of the average temperature input would not necessary modify the energy efficiency whereas the exergy efficiency has noticeable variations. Therefore, an increase in temperature does not necessarily mean an increase in energy efficiency. One can conclude that at this level, this indicator has slightly no direct effect on the efficiency of the drying system.

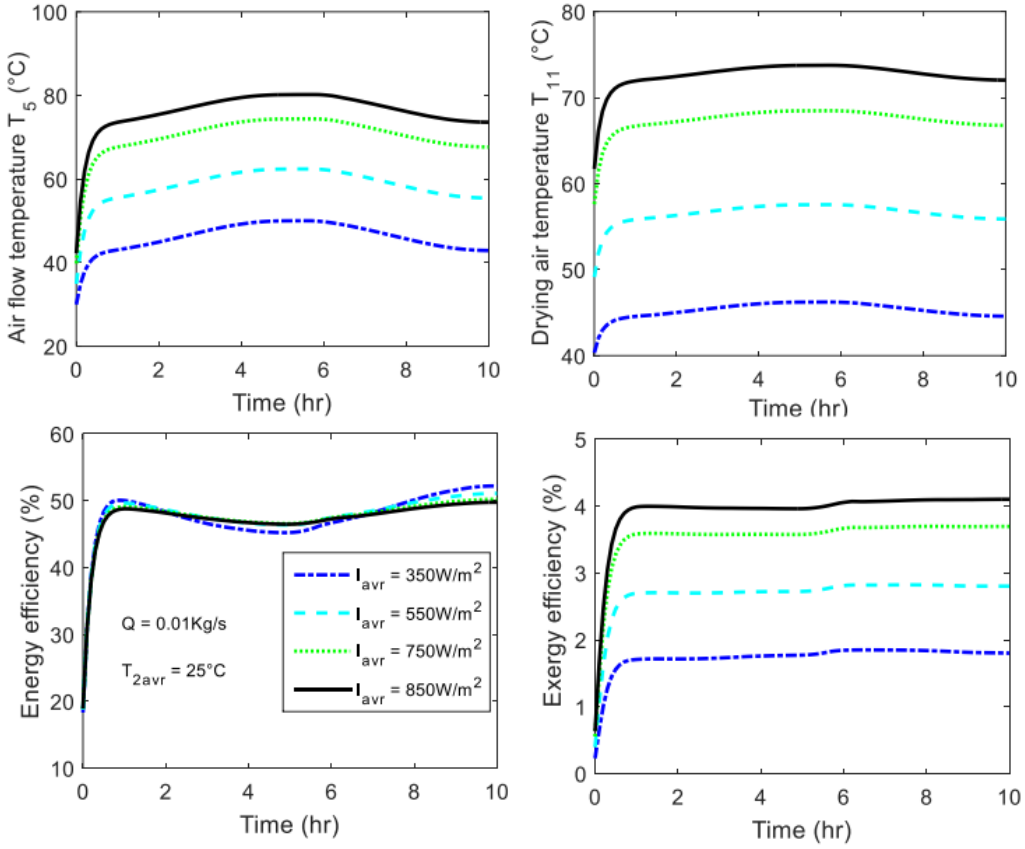

Figure 12. Effect of average solar intensity input on the performance of the drying system

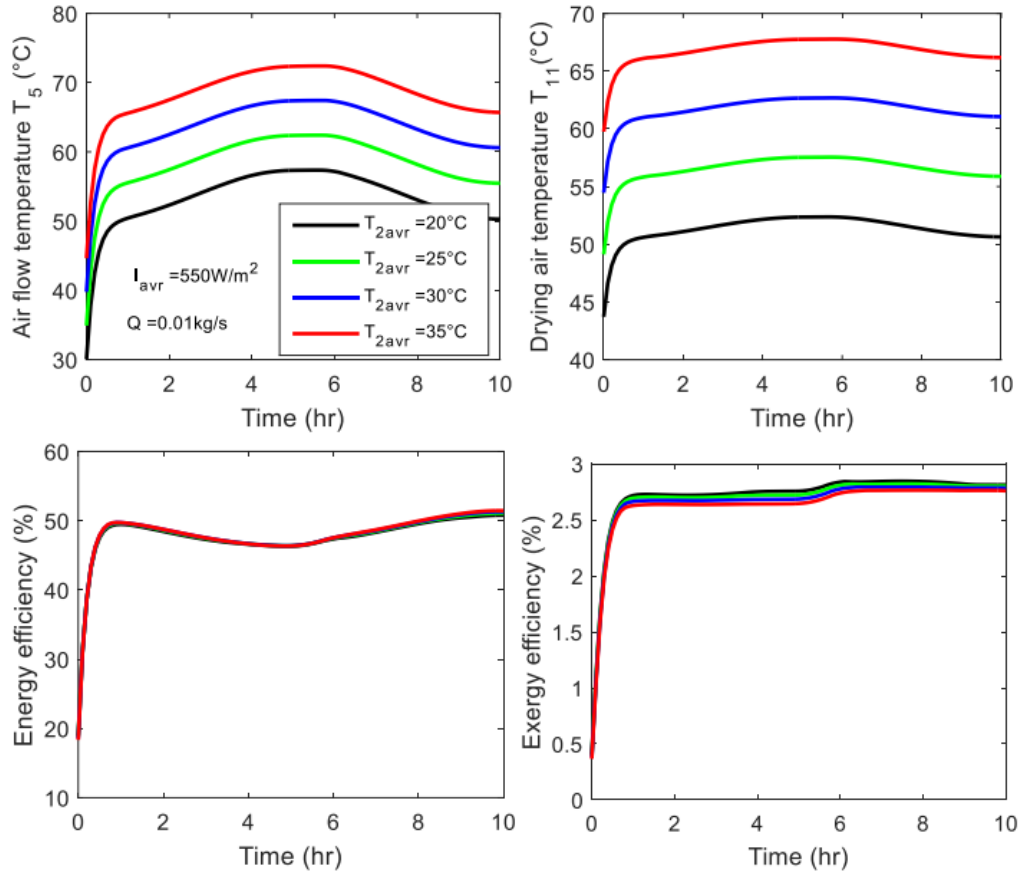

Figure 13. Effect of average temperature input on the performance of the drying system

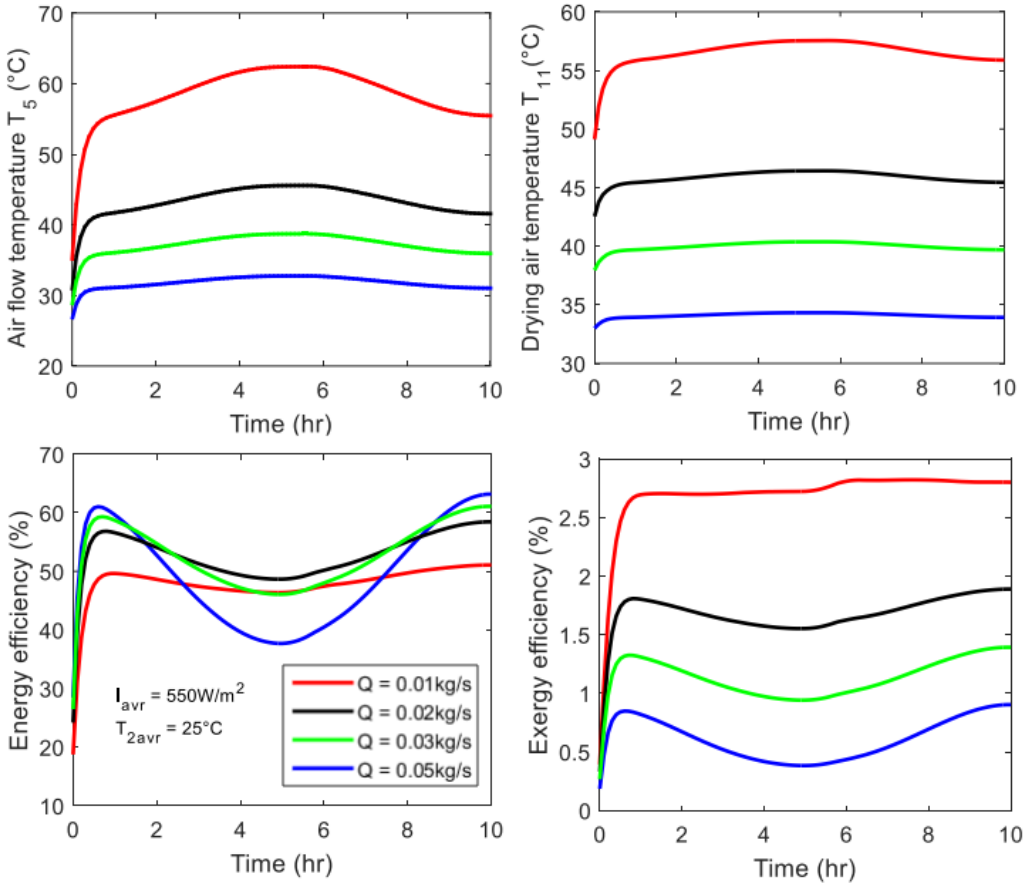

Figure 14. Effect of mass flow rate on the performance of the drying system.

The collector air temperature, the drying air in the dryer chamber, the instantaneous energy and exergy profiles are characterized in Figure 14 for various mass flow rate $Q = \{0.01, 0.02, 0.03, 0.05\} Kgs^{-1}$. Increasing of mass flow rate of the hot air causes a decrease of collector air temperature and consequently causes a decrease of drying temperature. In fact, when the heated air enters the drying chamber through the air inlet into the chamber, the heated air temperature will decrease to the chamber value. This is due to the convective exchange between the heated air and the sides of the drying milieu. The simulated results also show that contrary to the hourly temperature variation and exergy efficiency, the energy efficiency increases with the mass flow rate. This result is in great agreement with the energy performance tests performed by [27]. The predicted results are also consistent with the finding of [28]. However, it is interesting to note that at relatively high values of air flow rate, the energy efficiency exhibited misleading behaviors. Specifically for a value of Q greater than $0.02\, Kgs^{-1}$, the energy efficiency increases at time variations less to $2hr$ and the later starts to decrease until it minimum value which corresponds to a maximum point of inner air temperature variation, and then increases from this point to another maximum point. This result suggests an instability of the collector performance at this flow rate.

Finally, comparisons made using different values of temperature inputs and thermal waves on the predicting analysis were investigated to evaluate the difference between the simple conditions and real situations characterized by fluctuating boundary conditions. Figure 15 demonstrates the effect of the input temperature changes on prediction of temperature profile in solar dryer system. The results of the present method was studied for a value of the average temperature input $T_{avr} = 25$ °C. It was assumed also that $I_{avr} = 550W / m^2$ for a comparison with the predictions of Figure 13. From Figure 15, the observation on that the effect of ambient temperature change may cause significant variation of the outlet air temperature is possible. Nevertheless, the results of Figure 15 obtained, when applying a temperature transfer model to more complex conditions with the inputs air and solar radiation generated using more fluctuating curves, demonstrate that the travel time of the thermal responses has a direct effect on the output temperature and instantaneous thermal efficiency responses. Therefore, a slight increase and decrease in temperature does induce noticeable fluctuation of the instantaneous efficiency. In many studies, the predictions of energy and exergy performances of a solar drying system are generally determined using one-dimensional test equations [11,19,29]. However, the presented results reveal the space and time variability effects in predicting both the collector and dryer chamber facility elements temperature as well as their thermal performances. The two-dimensional simulations help to remove the previous one-dimensional test hypothesis and therefore, provide spatial and temporal variations of the basic physical phenomena involved in solar drying system. Such results can facilitate researchers in establishing a drying performance under different environmental and product load conditions.

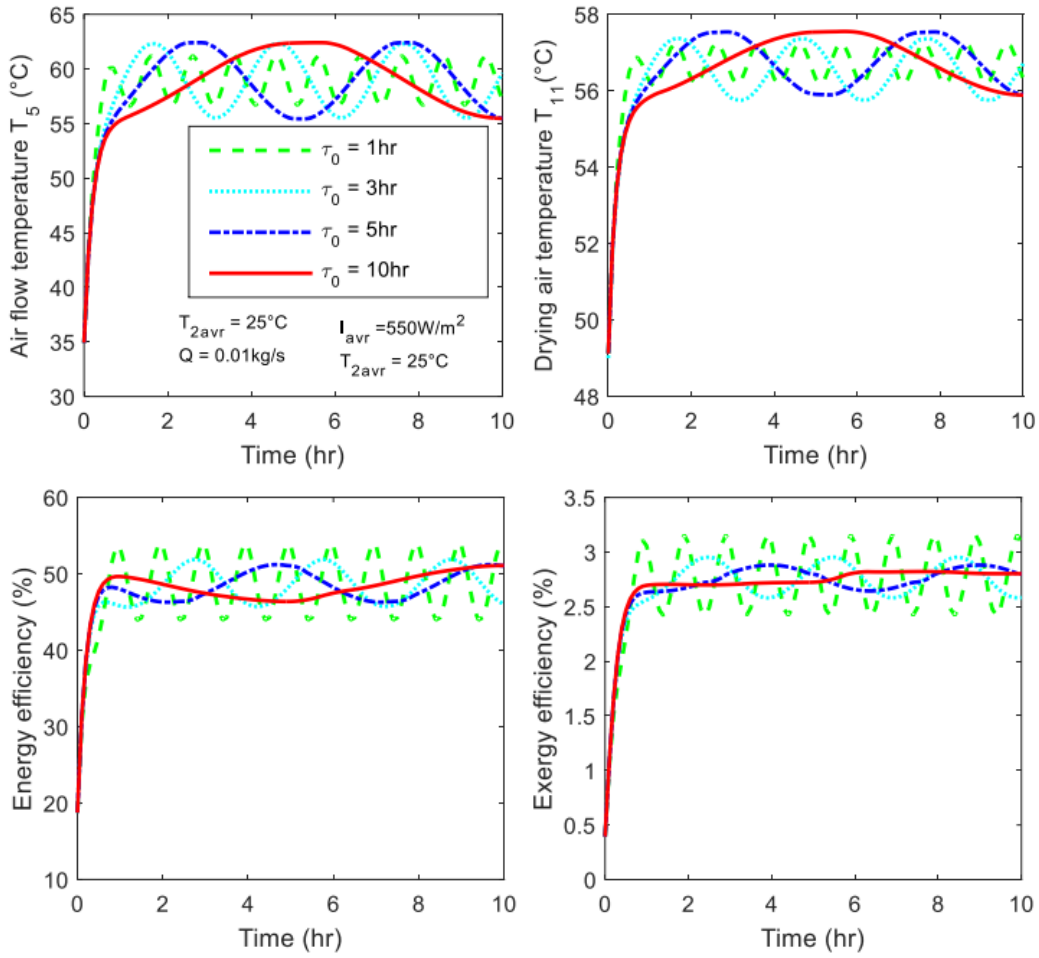

Figure 15. Effect of various temperature waves on the performance of the drying system

6. Conclusion

In this paper, an integrated two-dimensional mixed solar dryer model with double air pass was developed using a thermal network approach. The highly nonlinear differential equations obtained were solved iteratively using the finite difference method. The procedure produced the spatial and temporal distributions of the temperatures of both collector and drying compartment elements. The model presented gives a satisfactory agreement in that it offers accurate comparable results to previous existing one-dimensional solutions without the numerical complexity. The influences of space resolution, time variation, drying air flow rate, solar radiation intensity and average temperature inputs were revealed. The results of the numerical simulation show that the energy performance of the solar collector as well as the temperature of each element of the system increase with the space and time variations. The drying air temperature also decreases with the increase of the space node. It was demonstrated that the thermal efficiency decreases by decreasing the space variation. The energy efficiency increases also with the mass flow rate, while the exergy exhibits reverse behavior. Although, the average solar intensity input has minimal impact on the energy performance, the exergy efficiency decreases with decreasing the average solar radiation value. The developed strategy based on a simple equivalent electrical circuit analysis is part of an ongoing effort to improve characterization of the solar drying facility and to understand the physical phenomena involved in such system.

References

[1] Sulaiman, F., Abdullah, N, *Solar drying system for drying empty fruit bunches*, Journal of Physical Science, 2013, 75-93.

[2] Kumar, M., Sansaniwal, S.K., Khatak, P, *Progress in solar dryers for drying various commodities*, Renewable and Sustainable Energy Reviews, 2016, 346-360.

[3] Slimani, M.E.A., Amirat, M., Bahria, S., Kurucz, I., Sellami R, *Study and modeling of energy performance of a hybrid photovoltaic/thermal solar collector: Configuration suitable for an indirect solar dryer*, Energy conversion and management, 2016, 209-221.

[4] Vijayan, S., Arjunan, T.V., Kumar, A, *Mathematical modeling and performance analysis of thin layer drying of bitter gourd in sensible storage based indirect solar dryer*, Innovative food science & emerging technologies, 2016, 59-67.

[5] Lingayat, A., Chandramohan, V.P., Raju, V.R.K, *Design, development and performance of indirect type solar dryer for banana drying*, Energy Procedia, 2017, 409-416.

[6] Ekechukwu, O.V., Norton, B, *Review of solar-energy drying systems II: an overview of solar drying technology*, Energy conversion and management, 1999, 615-655.

[7] El-Sebaii, A.A., Shalaby, S.M, *Solar drying of agricultural products*: A review, Renewable and Sustainable Energy Reviews, 2012, 37-43.

[8] Pirasteh, G., Saidur, R., Rahman, S.M.A., Rahim, N. A, *A review on development of solar drying applications*, Renewable and Sustainable Energy Reviews, 2014, 133-148.

[9] Ong, K.S, *Thermal performance of solar air heaters: mathematical model and solution procedure*, Solar energy, 1995, 93-109.

[10] Njomo, D., Daguenet, M, *Sensitivity analysis of thermal performances of flat plate solar air heaters*, Heat and Mass Transfer, 2000, 1065-1081.

[11] Ramani, B.M., Gupta, A., Kumar, R, *Performance of a double pass solar air collector*, Solar Energy, 2010, 1929-1937.

[12] Languri, E.M., Taherian, H., Hooman, K., Reisel, J,*Enhanced double-pass solar air heater with and without porous medium*, International Journal of Green Energy, 2011, 643-65.

[13] Tchinda, R, *A review of mathematical models for predicting solar air heaters systems*, Renewable and Sustainable Energy Reviews, 2009, 1734-1759.

[14] Tian, Y., Zhao, C.Y, *A review of solar collectors and thermal energy storage in solar thermal applications*. Applied energy. 2013, 538-553.

[15] Tchinda, R, *Thermal behaviour of solar air heater with compound parabolic concentrator*, Energy Conversion and Management, 2008, 529-540.

[16] Tchinda, R., Ngos, N, *A theoritical evaluation of the thermal performance of CPC with flat one-sided absorber*,International Communications in Heat and Mass Transfer, 2006, 709-718.

[17] Banout, J., Kucerova, I., Marek S, *Using a double-pass solar drier for jerky drying*, Energy Procedia, 2012, 738-744.

[18] Hosseini, S.S., Ramiar, A., Ranjbar A.A, *Numerical investigation of natural convection solar air heater with different fins shape*, Renewable Energy, 2018, 488-500.

[19] Saxena, A., Varun, El-Sebaii, A.A, *A thermodynamic review of solar air heaters*, Renewable and Sustainable Energy Reviews, 2015, 863-890.

[20] Li, S., Wang, H., Meng, X., Wei, X, *Comparative study on the performance of a new solar air collector with different surface shapes*, Applied Thermal Engineering, 2016, 639-644.

[21] Duffie, J.A., Beckman, W.A, *Solar engineering of thermal process*, 2013, WILEY.

[22] Ghodbane, M., Boumeddane, B., Moummi, N., Largot, S., Berkane, H, *Study and numerical simulation of solar system for air heating*, Journal of Fundamental and Applied Sciences, 2016, 41-60.

[23] Simate, I.N, *Simulation of the mixed-mode natural-convection solar drying of maize*, Drying Technology, 2001, 1137-1155.

[24] Das, S, *Simulation of optimal exergy efficiency of solar flat plate collector*, Jordan Journal of Mechanical and Industrial Engineering, ISSN, 2016, 1995-6665.

[25] Gatea, A.A, *Performance evaluation of a mixed-mode solar dryer for evaporating moisture beans*, Journal of Agricultural Biotechnology and sustainable Development, 2011, 65-71.

[26] Chabane, F., Moummi, N., Benramache, S, *Experimental study of heat transfer and thermal performance with longitudinal fins of solar air heater*, J. Adv. Res, 2013, 183-92.

[27] Alobaid, M., Hughes, B., Heyes, A., Connar, D.O, *Determining the effect of inlet flow condition on the thermal efficiency of a flat plate solar collector*, Fluids, 2018, 1-17.

[28] Sun, W., Ji, J., Wei, H, *Influence of channel depth on the performance of solar air heaters*, Energy, 2010, 4201-4207.

[29] Hao, W., Liu, S., Mi, B., Lai, Y, *Mathematical modeling and performance analysis of a new hybrid solar dryer of lemon slices for controlling drying temperature*, Energies, 2020, 1-23.

[30] Mehta, P., Samaddar, S., Patel, P., Markam, B., Mait, S, *Design and performance analysis of a mixed mode tent-type solar dryer for fish-drying in coastal areas*, Solar Energies, 2018, 671-681.